Turbulence of a free surface

PHYSICAL REVIEW LETTERS

Turbulence of a Free Surface

Ralph Savelsberg and Willem van de Water

Physics Department, Eindhoven University of Technology, Postbus 513, 5600 MB Eindhoven, The Netherlands

We study the free surface of a turbulent channel flow, in particular, the relation between the statistical properties of the wrinkled surface and those of the velocity field beneath it. For an irregular flow shed off a vertical cylinder, surface indentations are strongly correlated with vortices in the subsurface flow. For fully developed turbulence this correlation is dramatically reduced. This is because the large eddies excite random capillary-gravity waves that travel in all directions across the surface. Both their predominant wavelength and their anisotropy are determined by the subsurface turbulence.

When observing a free surface of a turbulent stream one wonders what one sees: is its shape the imprint of the subsurface turbulence or does it depend on the dynamics of the surface itself? More precisely, the question is how the statistical properties of the turbulent crispations of the surface are linked to those of the turbulent velocity field beneath it. The small-scale roughness of the ocean's surface determines the exchange of heat and mass between the atmosphere and the ocean. These transport processes are crucial for the global distribution of momentum, heat, and chemical species. In a geophysical setting, the ocean surface is wrinkled by the wind and the turbulent motion of the flow beneath it. In this Letter we shall concentrate on the wrinkling of the free surface on a turbulent channel flow in still air.

The surface influences the turbulence beneath it. For a stress-free flat surface this has been considered in a seminal paper by Hunt and Graham [1], while some of the complications due to surface curvature were studied in [2–4]. There is a crucial difference between the turbulent velocity fluctuations in the bulk and those at the surface. First, the vertical velocities must vanish at the surface; second, while vortex tubes can never end inside the flow, they can end perpendicularly at the surface. This causes characteristic dimples of the surface above these vortices. It is tempting to associate each surface indentation with an attached vortex below it. Another surface wrinkling mechanism that has been suggested is through upwellings and downdraughts of parcels of fluid moving towards and away from the surface, concentrated in the strain regions between the vortices [5–7]. There is a whole range of scales in fully developed turbulence, which may thus be inherited by the surface crispations. As turbulence is a statistical phenomenon, the question is how to devise statistical quantities that can capture these phenomena. For example, for vortices attached to the surface one would expect a strong correlation between the surface height and the rotation of the velocity field just beneath it, while for upwellings and downdraughts the strongest correlation would be between the surface height and the strain.

We have developed a new precise and linear laser scanner to measure the surface gradient field [8]. By combining this with particle image velocimetry to measure the velocity field in a plane just beneath the surface, we will address the relation between the surface crispations and the velocity field. To our knowledge this is the first experiment that addresses the relation between fully developed turbulence of a flow and the turbulence of its free surface. Our experiments are done in a 7 m long and 0.3×0.3 m^2 cross-section water channel. Figure 1 shows a schematic picture of the channel, with the arrangement of the optical diagnostics, and a photograph of the turbulent free surface. Relatively strong homogeneous turbulence is generated by means of an active grid, as pioneered by Makita [9]. An active grid is a grid of rods with attached vanes, each of which can be rotated with a servo motor. By a judicious choice of the random rotation protocol, turbulence with tunable anisotropy and Reynolds number can be created. The typical mean flow velocity U is 0.3 m/s, with fluctuations $u = 0.023$ m/s, integral scale $L \approx 10^{-1}$ m, and Reynolds number $R_\lambda \approx 200$. Although an inertial range can be clearly recognized in spectra of velocity fluctuations in the bulk (not shown), our channel turbulence is weak in terms of its surface deformations. The Froude number, which compares the turbulent kinetic energy to the potential energy of the surface, is $\text{Fr} = u/(2gL)^{1/2} = 3 \times 10^{-2}$, while the Weber number, which is the ratio of the capillary energy density to the turbulent energy, is $\text{We} = u^2 L \rho/2\sigma = 0.3$, with σ the surface tension and ρ the density of water. Consequently, the surface wrinkles are shallow and rounded.

Homogeneous and isotropic turbulence is well documented, and the interaction with a free surface has been explored numerically [10]. Although the surface deformations are not very strong, there are highly nontrivial questions which must be answered first, before moving to more spectacular manifestations of free surface turbulence, such as breaking and frothing of the surface. For example, a question is how the spatial energy spectrum of the subsurface turbulent velocity field $E(k) \sim k^{-5/3}$ is reflected in the surface.
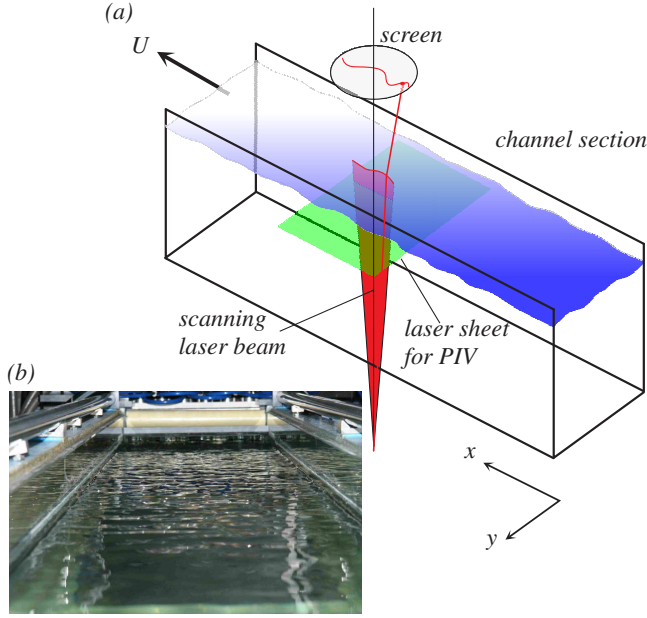
FIG. 1 (color online).   Turbulence inside a water channel flow wrinkles its free surface. (a) Schematic view of the experimental setup and the optical diagnostics to simultaneously measure the surface gradient field and the velocity field in a plane just below the surface. (b) Photograph of the turbulent free surface taken in the upstream direction. The turbulence is generated with the help of an active grid (not shown). The slope of the surface wrinkles is measured using the refraction of a laser beam that rapidly scans lines on the surface. The position of the refracted laser beam on a screen is measured with the help of a position-sensitive device. Simultaneously, the velocity field is measured through the displacement of particles that are illuminated by the laser sheet [particle image velocimetry (PIV)]. In the arrangement shown, the surface is scanned in the streamwise (x) direction. This is used for Figs. 4 and 5(a). Spanwise scans (Figs. 2 and 3) can be used to reconstruct 2D surfaces by employing Taylor's frozen turbulence hypothesis. A detailed account of the experimental method can be found in [8].

Although it is not turbulence, it is interesting to study the interaction of isolated coherent structures, such as jets [11], vortices, and vortex rings [12,13] with a free surface. These experiments are appealing, because they illustrate the intuitive connection between columnar vortices in the fluid and the surface dimples above their low-pressure cores. Figure 2 shows a result of such experiments in our water channel, where a surface-piercing vertical cylinder of 1.2 cm diameter sheds columnar vortices in a laminar flow. Side to side we show the measured surface gradient field $\nabla h(\boldsymbol{x})$ and the field $\boldsymbol{\xi} = -(\boldsymbol{u} \cdot \nabla)\boldsymbol{u}/g$, with g the acceleration of gravity. In the case of stationary, planar, and inviscid flow without surface tension, $\boldsymbol{\xi} = \nabla h$. Snapshots of these fields in Fig. 2 bear a striking resemblance, which can by quantified by the normalized correlation $C_{\xi,\nabla h}$ in terms of their inner product

$$C_{\alpha,\beta}(\boldsymbol{r}) = \langle \boldsymbol{\alpha}(\boldsymbol{x}+\boldsymbol{r},t) \cdot \boldsymbol{\beta}(\boldsymbol{x},t) \rangle / \langle \boldsymbol{\alpha} \cdot \boldsymbol{\alpha} \rangle^{1/2} \langle \boldsymbol{\beta} \cdot \boldsymbol{\beta} \rangle^{1/2},$$
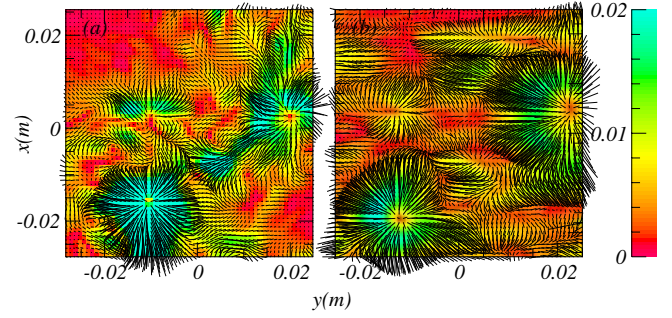

FIG. 2 (color online).   Relation between the velocity field and the free surface deformations of the turbulent flow behind a cylinder, demonstrated by two snapshots. The arrows indicate the vector fields, with the shading their magnitude. The mean flow velocity is 0.16 m/s, the cylinder diameter is 2 cm (Re = 1.9×10^3). (a) The normalized convective acceleration $\boldsymbol{\xi} = -(\boldsymbol{u} \cdot \nabla)\boldsymbol{u}/g$ computed from velocity fluctuations $\boldsymbol{u}$ that were measured in a plane 1 mm below the surface. (b) Measured surface gradient field ∇h. Two large vortices can be seen, where the fields $\boldsymbol{\xi}$ and ∇h are strikingly similar; elsewhere, they are different. Clearly, the field $\boldsymbol{\xi}$ picks out the large-scale depressions of the surface.

with the average $\langle \rangle$ done over $\boldsymbol{x}$ and over many ($\approx 10^3$) independent snapshots at times t and where the vector fields $\boldsymbol{\alpha}$ and $\boldsymbol{\beta}$ have zero mean. As expected, we find in Fig. 3 a strong correlation between $\boldsymbol{\xi}$ and ∇h, $C_{\xi,\nabla h}(0) = 0.4$. The question now is how these fields are related in the case of fully developed turbulence.

The surprising answer is that the connection between the quasistatic gradient field $\boldsymbol{\xi}$ and the measured gradient field ∇h is *an order of magnitude smaller* than that from the coherent vortices of Fig. 2, such that the connection decreases with increasing Reynolds numbers from $C_{\xi,\nabla h}(0) = 0.08$ at $R_\lambda = 126$ to $C_{\xi,\nabla h}(0) = 0.04$ at $R_\lambda = 173$. The convective acceleration field $\boldsymbol{\xi}$ can be separated in a strain $\boldsymbol{S}$ and rotation $\boldsymbol{\Omega}$ part, $\boldsymbol{\xi} = \boldsymbol{\xi}_S - \boldsymbol{\xi}_\Omega = \boldsymbol{u} \cdot (\boldsymbol{S} - \boldsymbol{\Omega}/2)/g$. The correlation between the surface gradient field and the rotation part is sensitive to surface connections consisting of dimples above attached vortex cores, while the correlation with the strain part is sensitive to upwellings and downdraughts. For the vortex field shed from the cylinder (see Fig. 2) we find that strain and rotation are equally strongly correlated. However, for fully developed turbulence, we find that the gradient field is correlated most strongly with the strain $\boldsymbol{S}$. [$C_{\xi_S,\nabla h}(0) \approx 2C_{\xi_\Omega,\nabla h}(0)$.] Clearly, the intuitively appealing picture of the surface deformations consisting of dimples above random turbulent eddies is too simple. Adding surface tension to the hydrostatic field ∇h, and computing the correlation between $\boldsymbol{\xi}$ and $\nabla h - \frac{\sigma}{\rho g}\nabla(\nabla^2 h)$, where the surface curvature was estimated from quadratic fits to the measured surface profile, does not alter our conclusions. The dramatic loss of coherence between the velocity field and the surface above the turbulence suggests that the surface possesses dynam-
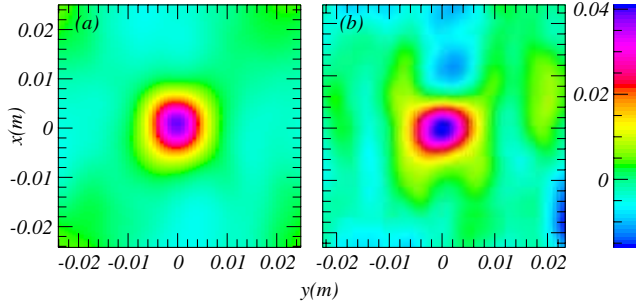
FIG. 3 (color online).   Correlation $C_{\xi,\nabla h}$ between the convective acceleration field $\boldsymbol{\xi}$ and the surface gradient field ∇h. (a) For a random surface behind a vertical cylinder, $\langle \nabla h \cdot \nabla h \rangle^{1/2} = 6 \times 10^{-3}$. (b) For a fully developed turbulent surface, $\langle \nabla h \cdot \nabla h \rangle^{1/2} = 3 \times 10^{-2}$. The intensity scale of (a) is 10 times the shown scale of (b): the maximum correlation for (a) is $C_{\xi,\nabla h}(0) = 0.4$, whereas for (b) $C_{\xi,\nabla h}(0) = 0.04$.

ics of its own. More about this dynamical behavior can be learned from the energy spectrum $E(k_x, \omega)$ of the surface gradient field,

$$E_{x,y}(k_x, \omega) = \left\langle \left| \iint e^{ik_x x + i\omega t} \nabla_{x,y} h(x, y = 0, t) dx dt \right|^2 \right\rangle.$$

The measured spectrum $E_x(k_x, \omega)$ in Fig. 4 shows a ridge at $\omega = k_x U$, corresponding to structures traveling with the mean flow velocity. However, those are outweighed by structures that approximately satisfy the Doppler-shifted dispersion relation of capillary-gravity waves, $\omega = \omega_d(k) \pm Uk$, with $\omega_d(k) = (gk + \sigma k^3/\rho)^{1/2}$.

Figure 4(c) also shows the wave number spectrum $E_x(k_x) = \int_0^\infty E_x(k_x, \omega) d\omega$ of the surface. The spectral energy drops extremely steeply with increasing wave number k, $E(k) \sim k^{-6}$. Weak-wave turbulence theory [14] predicts Kolmogorov-like spectra for the elevation of weakly nonlinear surface waves. For the surface gradient field of capillary waves, $E(k) \sim k^{-11/4}$, which decays much slower than our measured spectra. However, our strongest nonlinearity is $\langle \nabla h \cdot \nabla h \rangle^{1/2} = 3 \times 10^{-2}$, while weak-wave turbulence starts at nonlinearity ≈ 0.1.

The companion space-time correlation function in Fig. 5, which emphasizes the large energetic scales, shows structures on the surface which are traveling with velocity $U + \upsilon$, and $U - \upsilon$, respectively, with $\upsilon \approx 0.38$ m/s, as opposed to structures that move with the mainstream velocity. Similarly, the spanwise space-time correlation function in the *spanwise* direction shows structures traveling with $\upsilon = \pm 0.38$ m/s. The observed propagation velocity $\upsilon = 0.38$ m/s corresponds to the phase velocity of capillary-gravity waves with wavelength $\lambda = 0.089$ m, which can be compared very well to the (longitudinal) integral length scale $L = 0.085$ m of the subsurface velocity field. Because of the waves, an observation of the moving texture of a turbulent free surface tells the mean flow velocity U only *indirectly*: in the streamwise direction
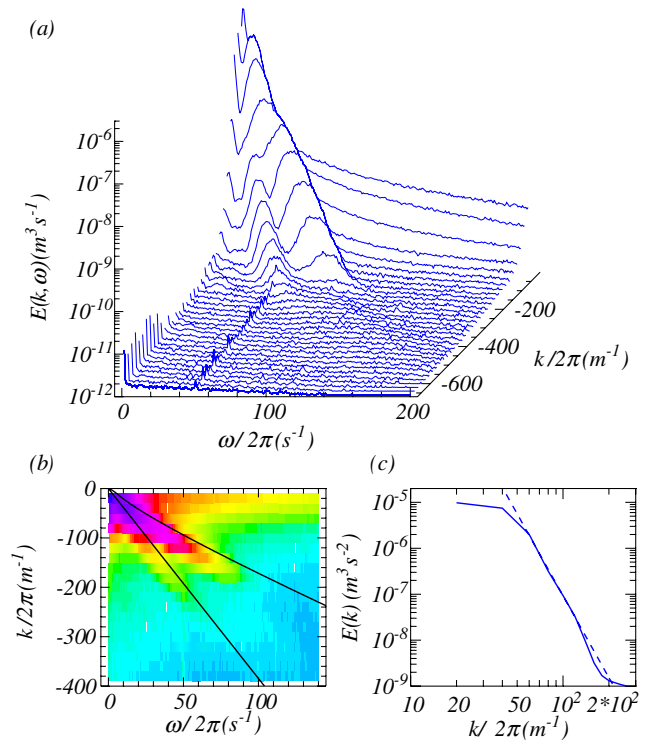

FIG. 4 (color online).   Energy spectrum of the surface gradient measured along a line in the streamwise direction. (a) Surface plot, (b) corresponding shading plot; the shading scale is logarithmic. Full lines show convection by the mean flow, $\omega = kU$, and the blueshifted Doppler relation for capillary-gravity waves. Redshifted waves have very low frequencies and occur at positive wave numbers (not shown). (c) Full line: wave number spectrum $E_x(k_x) = \int_0^\infty E_x(k_x, \omega) d\omega$; dashed line: fit $E_x(k) \propto k^{-6}$.

the surface texture moves up and downstream with a velocity that far exceeds the mean velocity of the flow.

From a measurement of the spatial correlation function of $\nabla_x h$ and $\nabla_y h$, in both x and y directions, it appears that the surface crispations are isotropic if the subsurface turbulence is isotropic and anisotropic if the bulk turbulence
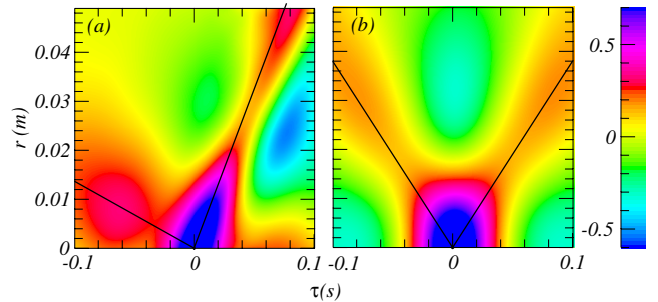

FIG. 5 (color online).   Space-time correlation functions $C(r, \tau) = \langle \nabla h_\alpha[(r + x)\boldsymbol{e}_\alpha, t + \tau] \cdot \nabla h_\alpha(x\boldsymbol{e}_\alpha, t) \rangle / \langle \nabla h_\alpha \cdot \nabla h_\alpha \rangle$. (a) Streamwise ($\alpha = x$), full lines: $r = U \pm \upsilon\tau$, with $\upsilon = 0.38$ m/s. (b) Spanwise ($\alpha = y$), full lines: $r = \pm \upsilon\tau$, with $\upsilon = 0.38$ m/s.
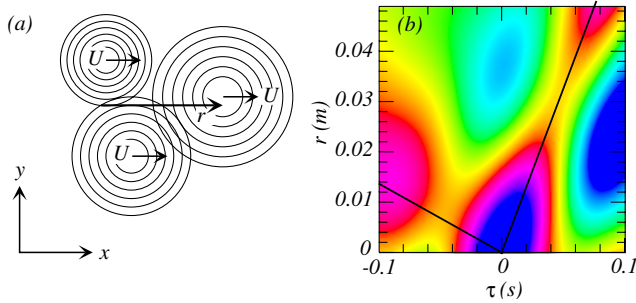
FIG. 6 (color online).   (a) A simple model in which sources are randomly sprinkled on the surface which radiate capillary-gravity waves from Gaussian initial depressions, $h_0(r) = -\exp(-r^2/r_0^2)$, with $r_0 = 0.021$ m. The entire surface moves with the mean velocity $U = 0.25$ m/s. (b) Streamwise correlation function $C(r, \tau)$ of $\nabla_x h$; full lines: $r = U \pm v\tau$, with $v = 0.38$ m/s. The shading scale is the same as that of Fig. 5.

is made anisotropic. Thus, the free surface above a turbulent flow mainly consists of capillary-gravity waves that spawn from everywhere on the surface and that travel in all directions across the surface. This explains why the spectrum of Fig. 4(b) is only approximately the Doppler-shifted spectrum of plane waves traveling up and downstream: only the waves that are seen head-on by the detector experience the full Doppler shift.

This simple picture is illustrated by a model calculation, in which the surface is randomly sprinkled by sources at $x_i(t)$ that emit circular waves from an initial Gaussian depression $h_0(r) = -\exp(-r^2/r_0^2)$. All sources have radius r_0 and are advected by the mean velocity. Each source contributes ∇h^i to the gradient field, with $\nabla h^i(r, t) = -\frac{x - x_i(t)}{r} \int_0^\infty k^2 F(k) J_1(kr) \cos[\omega(k)t] dk$, $\quad r = x - x_i(t)$, and $F(k)$ the Fourier-Bessel transform of the initial profile, $F(k) = r_0^2 \exp(-k^2/k_0^2)/8\pi$, with $k_0 = 2/r_0$. The resulting space-time correlation function in Fig. 6 bears a striking resemblance to the experimental result of Fig. 5. With $r_0 = 0.021$ m, we find the same convection velocity as in the experiment. Clearly, the characteristic wavelength of the Gaussian spectrum $\lambda = 2\pi/k_0 = \pi r_0 = 0.067$ m points to the large-scale structure of the subsurface velocity field, but profound questions remain about the precise relation between the statistics of the surface crispations and the large-scale statistics of the subsurface turbulent velocity field.

Let us repeat that at integral scales $l = L$, the surface energy σ/l is smaller than the kinetic energy $\rho u(l)^2/2$ of the subsurface turbulence. The imbalance worsens for decreasing scales where the surface energy increases but where the turbulence energy decreases as $l^{2/3}$. Therefore, the surface is most likely excited by the largest subsurface turbulence scales only. In our experiment the root-mean-square turbulent velocity $u = 0.023$ m/s is much smaller than the minimum phase velocity of capillary-gravity waves on water ($v_{f_{\min}} = 0.23$ m/s). Surprisingly, however, the surface responds with capillary-gravity waves. When u approaches $v_{f_{\min}}$, the possibility exists of a *resonant* excitation of surface waves by eddies whose size matches the wavelength and whose velocity matches the corresponding phase velocity [15]. This opens up a new regime in which surface crispations are no longer excited by integral-scale eddies only. However, an increase of an order of magnitude in u in grid-generated turbulence implies an increase of 3 orders of magnitude in injected power in our experiment, which is unfeasible.

In conclusion, the wrinkled free surface above a turbulent channel flow is dominated by random capillary-gravity waves. From the subsurface turbulence the free surface inherits the low wave number fluctuations: namely, its integral length scale and its anisotropy. At higher wave numbers the surface has a life of its own. This reduces the correlation between the surface gradient field and the subsurface velocity field. We find that it is an order of magnitude weaker than predicted by numerical simulations [3].

[1] J. Hunt and J. Graham, J. Fluid Mech. **84**, 209 (1978).
[2] T. Sarpkaya, Annu. Rev. Fluid Mech. **28**, 83 (1996).
[3] W.-T. Tsai, J. Fluid Mech. **354**, 239 (1998).
[4] L. Shen, X. Zhang, D. Yue, and G. Triantafyllou, J. Fluid Mech. **386**, 167 (1999).
[5] M. Brocchini and D. Peregrine, J. Fluid Mech. **449**, 225 (2001).
[6] S. Kumar, R. Gupta, and S. Banerjee, Phys. Fluids **10**, 437 (1998).
[7] R. Nagaosa, Phys. Fluids **11**, 1581 (1999).
[8] R. Savelsberg, A. Holten, and W. van de Water, Exp. Fluids **41**, 629 (2006).
[9] H. Makita, Fluid Dyn. Res. **8**, 53 (1991).
[10] B. Perot and P. Moin, J. Fluid Mech. **295**, 199 (1995).
[11] D. Walker, C.-Y. Chen, and W. Willmarth, J. Fluid Mech. **291**, 223 (1995).
[12] M. Gharib, Appl. Mech. Rev. **47**, S157 (1994).
[13] M. Gharib and A. Weigand, J. Fluid Mech. **321**, 59 (1996).
[14] V. Zakharov, V. L'Vov, and G. Falkovich, *Kolmogorov Spectra of Turbulence* (Springer-Verlag, Berlin, 1992).
[15] O. Phillips, J. Fluid Mech. **2**, 417 (1957).